CARDIFF UNIVERSITY
PRIFYSGOL CAERDYDD

ORCA – Online Research @ Cardiff

This is an Open Access document downloaded from ORCA, Cardiff University's institutional repository:https://orca.cardiff.ac.uk/id/eprint/77806/

This is the author's version of a work that was submitted to / accepted for publication.

Citation for final published version:

Kennedy, Alan, Farnsworth, Alexander, Lunt, Daniel, Lear, Caroline Helen and Markwick, Paul 2015. Atmospheric and oceanic impacts of Antarctic glaciation across the Eocene–Oligocene transition. Philosophical Transactions of the Royal Society A: Mathematical Physical and Engineering Sciences 373 (2054) , 20140419. 10.1098/rsta.2014.0419

Publishers page: http://dx.doi.org/10.1098/rsta.2014.0419

Please note:
Changes made as a result of publishing processes such as copy-editing, formatting and page numbers may not be reflected in this version. For the definitive version of this publication, please refer to the published source. You are advised to consult the publisher's version if you wish to cite this paper.

This version is being made available in accordance with publisher policies. See http://orca.cf.ac.uk/policies.html for usage policies. Copyright and moral rights for publications made available in ORCA are retained by the copyright holders.

Atmospheric and oceanic impacts of Antarctic glaciation across the Eocene-Oligocene transition

Kennedy, A.T.; Farnsworth, A.; Lunt, D.J.; Lear, C.H.; Markwick, P.J.

Abstract

The glaciation of Antarctica at the Eocene-Oligocene transition (~34 million years ago) was a major shift in the Earth's climate system, but the mechanisms that caused the glaciation, and its effects, remain highly debated. A number of recent studies have used coupled atmosphere-ocean climate models to assess the climatic effects of Antarctic glacial inception, with often contrasting results. Here, using the HadCM3L model, we show that the global atmosphere and ocean response to growth of the Antarctic ice sheet is sensitive to subtle variations in palaeogeography, using two reconstructions representing Eocene and Oligocene geological stages. The earlier Stage (Eocene; Priabonian), which has a relatively constricted Tasman Seaway, shows a major increase in sea surface temperature over the Pacific sector of the Southern Ocean in response to the ice sheet. This response does not occur for the later Stage (Oligocene; Rupelian), which has a more open Tasman Seaway. This difference in temperature response is attributed to reorganisation of ocean currents between the stages. Following ice sheet expansion in the earlier stage, the large Ross Sea gyre circulation decreases in size. Stronger zonal flow through the Tasman Seaway allows salinities to increase in the Ross Sea, deep-water formation initiates and multiple feedbacks then occur amplifying the temperature response. This is potentially a model dependent result, but it highlights the sensitive nature of model simulations to subtle variations in paleogeography, and highlights the need for coupled ice sheet-climate simulations to properly represent and investigate feedback processes acting on these timescales.

Key words
Eocene-Oligocene transition, Antarctic glaciation, palaeoclimate, palaeogeography, modelling, feedbacks.

1. Introduction

The Eocene-Oligocene transition (EOT), ~34 million years ago (34 Ma), represents one of the major climatic transitions in the past 65 million years (Zachos *et al*., 2008). A steady decline in temperatures from ~50 to ~34 Ma culminated in the rapid expansion of permanent ice over Antarctica (Zachos *et al*., 2001; Katz *et al*., 2008; Lear *et al*., 2008). Previous work has generally focused on two main causes of the EOT: the CO_2 hypothesis and the ocean-gateway hypothesis. The first suggests the global decline in CO_2 (itself due to increased biological uptake and carbon cycling, and/or increased silicate weathering, and/or decreased volcanic emissions) caused the drop in global temperature (Zachos & Kump, 2005) which, due to polar amplification through ice-albedo and topographical feedbacks, led to the growth of the Antarctic ice sheet (AIS; e.g. DeConto & Pollard, 2003; Pearson *et al*., 2009; Pagani *et al*., 2011; Foster & Rohling, 2013). The second hypothesis is that the opening of the ocean passages around Antarctica – the Drake Passage (DP) between South America, and Tasman Seaway (TS) between Australia – allowed for the initiation of the Antarctic circumpolar current (ACC) which reduced poleward heat transfer and so led to glacial inception (Kennett, 1977; Sijp & England, 2004). Although there is geological and modelling evidence for both hypotheses, recently an increasing body of evidence has given precedence to falling atmospheric CO_2 as being the chief driver of the EOT, with the precise timing influenced by orbital variations (e.g. DeConto & Pollard, 2003; Huber *et al*., 2004; Coxall *et al*., 2005; Pearson *et al*., 2009; Pagani *et al*., 2011; Sijp *et al*., 2011 Lefebvre *et al*., 2012; Goldner *et al*., 2014; Ladant *et al*., 2014).

The remainder of this section summarises proxy records of palaeoclimate through the EOT, the results of a number of recent modelling studies exploring the effects of Antarctic ice sheet expansion on global climate, and develops the motivation for our own work.

By way of introduction, the EOT is recorded as a two-stepped, orbitally-paced, ~1.5 ‰ increase in deep ocean benthic foraminiferal oxygen isotope ($\delta^{18}O$) records (Kennett & Shackleton, 1976; Zachos *et al*., 1996; Coxall *et al*., 2005). Benthic and low latitude planktonic $\delta^{18}O$ changes are shown in Figure 1a. These records reflect both an increase in continental ice volume and a decrease in ocean temperature, due to concentration of ^{16}O in ice sheets by the hydrological cycle and isotopic fractionation during the calcification process respectively. Attempts to deconvolve the EOT $\delta^{18}O$ increase into its ice volume and temperature components require the use of palaeotemperature proxies such as benthic foraminiferal Mg/Ca ratios. Further uncertainties arise in using Mg/Ca ratios due do a simultaneous ~1 km deepening of the calcite compensation depth (Lear *et al*., 2004; Coxall *et al*., 2005; Lear *et al*., 2010; Peck *et al*., 2010; Pusz *et al*., 2011), as well as error in the Mg/Ca value chosen for Eocene-Oligocene seawater and its relationship with foraminiferal Mg/Ca. Uncertainty due to calcite compensation depth deepening is reduced by using continuously paired $\delta^{18}O$ and Mg/Ca records, such as those from Tanzania Drilling Program (TDP; Pearson *et al*., 2008; Lear *et al*., 2008). Additionally, the long residence times of Mg and Ca in the oceans (~10 Myr and ~1 Myr respectively) mean that calculated changes in temperature and $\delta^{18}O_{sw}$ across the transition are more robust than absolute estimates (Lear *et al*., 2008).

The first step in the $\delta^{18}O$ record (Figure 1a) predominantly reflects an ocean cooling in low latitude surface waters with a small component of ice volume growth (~0.2‰ $\delta^{18}O_{sw}$ equivalent; Lear *et al*., 2008). Cooling ranges from ~2.5 °C at TDP (Lear *et al*., 2008) to ~3-4 ˚C in a multi-proxy Gulf of Mexico record (Wade *et al*., 2012; note, however, that the second step is absent for this record). High latitude Mg/Ca records from the Kerguelen Plateau in the Southern Ocean (SO) also suggest a 2.5 °C cooling (Bohaty *et al*., 2012). The second step is dominated by an increase in ice volume (~0.4‰

$\delta^{18}O_{sw}$ equivalent), supported by a decrease in the low latitude TDP benthic-planktonic foraminiferal $\delta^{18}O$ gradient, as shown in Figure 1b. This is interpreted as reflecting global sea level fall as ice sheets advanced (Lear *et al*., 2008). There is also evidence for some further deep ocean cooling at the second step (totalling ~4 ˚C across the EOT) that is not present at the surface in low latitude TDP records (assuming minimal change in local surface salinity), as shown in Figure 1c (Pearson *et al.*, 2008; Lear *et al*., 2008; Coxall *et al*., 2005). A multi-site study using the TEX_{86} and $U^{K'}_{37}$ organic temperature proxies suggests there was a heterogeneous SST response at the EOT (Liu *et al*., 2009). Modelling results, however, are generally consistent with an overall deep-water cooling of ~4 °C and an overall increase in ice volume of 10-30 x 10^6 km^3 across the EOT (Liu *et al*., 2009).

Modelling is important in fingerprinting the driving mechanisms behind the EOT. Although often studies have chiefly been concerned with the trigger of glacial inception or the ACC, the range of results and simulation setups in the literature pose interesting questions about the role of palaeogeography and the presence of the AIS on global climate. Indeed, several modelling studies in the past two years have explored the effects of AIS expansion on global climate, and we summarise these here:

Goldner *et al*. (2013) simulated the climate of the modern-day and the Eocene, both with and without an AIS, using the NCAR CESM1.0 global climate model with a slab ocean. They find a contrasting response to the formation of the AIS between the modern and Eocene, which they attributed to differing cloud feedbacks. In the Eocene the feedback is negative, causing warming when the AIS forms, whereas the cloud feedback is weakly positive in the modern. They acknowledge that this result is likely to be model dependent.

Building on their earlier work, Goldner *et al*. (2014) used the same model (NCAR CESM1.0) but with a more realistic three-dimensional fully dynamic ocean and also included simulations with different CO_2 concentrations. They suggest that changes found in the high-latitude ocean core records at the EOT, previously explained only by the gateway hypothesis and not the CO_2 hypothesis, could be an outcome of the formation of the AIS itself. The formation of the AIS increased the meridional pressure gradient around the continent, in turn increasing the surface winds that affect the surface mixing in the Southern Ocean. This led to enhanced northward transport of Antarctic Intermediate Water (AIW) and invigorated Antarctic Bottom Water (ABW) formation. Around the Antarctic coastline, the SST was found to have areas of both increases (in the Indian Ocean sector) and decreases (in the Pacific and Atlantic sectors).

Knorr and Lohmann (2014) carried out a similar study with a fully coupled climate model (ECHAM5/MPIOM) with a 3D ocean, but looked at a different time period and hence palaeogeography, that of the Middle Miocene ~14 Ma. Their work indicates that the addition of the AIS causes a contrasting response in the SST around Antarctica to that of Goldner *et al*. (2014), with strong warming in the Atlantic and Indian Ocean sectors (particularly in the Weddell Sea) and mild cooling in the Pacific sector. These changes in SST between glaciated and unglaciated simulations they attribute to winds affecting ocean circulation, deep-water formation and sea ice cover.

Hill *et al*. (2013) present results using the same climate model as used in this paper, HadCM3L. They look at several scenarios and palaeogeographies (the Rupelian and Chattian stages, and pre-industrial modern) with differing boundary conditions (AIS presence and an open or closed DP, but not every combination thereof). Although the Rupelian is also used in the current study, the palaeogeography has since been updated (for example in West Antarctica). They suggest that although the ACC starts to initiate with the opening of the DP and the TS, an ACC of present-day strength does not develop

until after the Chattian due to the proximity of the Australian continent to Antarctica prior to this time. They argue this result is consistent with geologic data (Pfuhl & McCave, 2005; Lyle *et al*., 2007).

There are several recurring points that emerge from these studies. Firstly, the response of the climate system to an expansion in Antarctic ice appears to vary significantly between models. However, it is also possible that the results are strongly dependent on the time period (i.e. palaeogeography) examined - Goldner *et al*., 2014, Knorr & Lohmann, 2014, and Hill *et al*., 2013 all examine differing time periods and/or palaeogeographies. The significance of palaeogeography cannot be underestimated, particularly when there is such large debate over the timings of key events such as the opening of the DP (Barker & Thomas, 2004; Stickley *et al*., 2004; Barker *et al*., 2007). Additionally, it seems that the effect of changing ocean circulation is a significant driver of the global climate at the EOT, even if it was not the ultimate trigger of Antarctic glaciation (Goldner *et al*., 2014; Lefebvre *et al*., 2012; Sijp *et al*., 2011 etc.). Palaeogeography, ocean circulation, CO_2 and climatic change are all therefore inter-connected and each warrants a complete understanding at this major climatic shift.

Here, we model and describe the global atmospheric and oceanic response to the glaciation of Antarctica in the HadCM3L model and compare this to previous studies. This experiment may therefore be indicative of the climatic changes that occurred during the second 'ice growth' step of the EOT. We do this for two successive periods over the EOT: the Priabonian during the Eocene (~38-34 Ma), and the Rupelian during the Oligocene (~34-28 Ma). These stages have subtly different palaeogeographies; for example the Tasman Seaway is wider in the Rupelian than the Priabonian in our reconstructions (see next section). We do not attempt to model the inception of glaciation in a transient simulation, like the studies of DeConto & Pollard (2003) or Ladant *et al*. (2014), but instead, through steady-state simulations we aim to explore the importance of the palaeogeography on the regional and global response to glaciation, and the associated feedbacks. Our experimental design is briefly outlined in section 2, descriptive results in section 3, analysis and discussion of the physical mechanisms and implications in section 4, and conclusions and future direction of work in section 5.

2. Experimental design

To investigate the model sensitivity to AIS expansion and subtle variations in the palaeogeography, the model HadCM3L was run towards a steady state using high-resolution palaeogeographic reconstructions of the stages, with and without reconstructed ice sheets. HadCM3L is a fully coupled atmosphere-ocean general circulation model (GCM; Cox *et al*., 2001). HadCM3L is a lower-resolution version (3.75 ° × 2.5 °) of the HadCM3 model (Gordon *et al*., 2000), with a few changes in parameterisations (see Cox *et al*., 2001 and Jones, 2003 for example) compared to HadCM3. No ice sheet model was included; the AIS was simply prescribed with an appropriate land surface albedo and topography. The ice sheet topography, as well as global bathymetry and topography was supplied by Getech Plc. at a 0.25 ° resolution. These were based upon tectonic, lithologic and fossil studies and DSDP/ODP deep-sea data (Markwick, 2007). The principle ice sheet used is a reconstruction for the Rupelian and is similar to the full modern extent (~17 x 10^6 km^3 in size). A smaller ice sheet was also used for cross-examination, similar to only the East AIS (EAIS; ~14 x 10^6 km^3 in size). These reconstructions are shown in Figure 2, and experiments listed in Table 1.

Model spin-up was carried out in four phases consistently across the simulations. First, in Phase 1, the model was initialised with pre-industrial CO_2 levels and a zonally symmetric SST and deep ocean distribution, uniform vegetation and the different ice-free palaeogeographies, and run for 50 years. In

Phase 2, the vegetation model TRIFFID (Cox, 2001) was activated, CO_2 was increased to four times pre-industrial, the prescribed ozone concentration was adjusted (Lunt *et al*., 2007), and the model run for 319 years. In Phase 3, prescribed lakes were added to the land surface and the ice sheet added in simulations requiring it, and the model run for 53 years. Finally, in Phase 4, barotropic flow in the ocean is calculated (prior to this point, only the baroclinic component was calculated), the CO_2 is reduced to two times pre-industrial (560 ppm), and for ice sheet sensitivity simulations the ice sheet is adjusted (differences are noted in Table 1). This final phase is run for 1000 years. This combined spin-up of 1422 years produces quasi-stable results for atmospheric and surface ocean characteristics as deep as 670 m, as shown in Supplementary Figure 1. There is still, however, a trend in deep ocean temperatures >1000 m and so these are not the focus of this study. More details of the experimental design can be found in Inglis *et al*. (in press), and Lunt *et al*. (in prep).

Table 1: Key details of each model simulation carried out. Those experiments marked with a * are the principle experiments around which the results and discussion are based.

Simulation name	Palaeogeography	Ice sheet configuration	Spin-up phase with final ice sheet state	CO_2
PriNO*	Priabonian	Ice-free	3	560 ppm
PriEAIS	Priabonian	East Antarctic ice only	4	560 ppm
PriFULL*	Priabonian	Full Antarctic ice sheet	4	560 ppm
RupNO*	Rupelian	Ice-free	3	560 ppm
RupEAIS	Rupelian	East Antarctic ice only	4	560 ppm
RupFULL*	Rupelian	Full Antarctic ice sheet	3	560 ppm

There are a number of points we would like to note about the methodology for clarity. Firstly, because the land-sea and ice masks do not align exactly between the stages, a small number of grid cells which should be prescribed as 'ice' lie off the continental margin of Antarctica during the Priabonian. It was deemed more important not to influence the bathymetry by changing the land-sea mask and so these occasional cells of ice sheet were omitted. Secondly, adjustments to the ice sheet states for sensitivity simulations (PriEAIS, PriFULL and RupEAIS) were made only in the fourth Phase of spin-up. These three simulations therefore have a slightly shorter spin-up (by 53 years) with their final ice sheet configuration than RupFULL. Thirdly, in our HadCM3L setup, the standard deviation of topography (used in the gravity-wave drag scheme) is estimated as a constant factor of the topographic height. This is a fair assumption over mountainous regions, but exaggerates the standard deviation over the AIS, potentially altering atmospheric dynamics. Fourthly, the solar constant varies fractionally between the stages (1360.86 and 1361.35 kW m^{-2} for the Priabonian, and Rupelian respectively). It is not believed that any of these points should have a major impact on the findings of the study.

Finally, the solution of the barotropic component of ocean circulation requires the user to define islands around which the net flow can be non-zero. Any continent and its coastline that is not defined as an island is assigned a barotropic stream function value of 0. For the Rupelian we define Australia, South America and Antarctica to be islands in this sense, whereas in the Priabonian, with a more constricted TS, we only define Australia and South America as islands. As such, there is zero net flow around the Antarctic coastline in the Priabonian, despite the presence of a (albeit small) TS. By

assigning the same value of stream function to Antarctica as the Eurasian and North American continents we provide a coupling between the Southern Ocean and tropical Pacific gateways in the Priabonian that is not present in the Rupelian (see Figure 5, shown later). This should not have a major effect on flow through the TS or the high latitude response during the Priabonian, but may potentially affect the climate response at low latitude.

3. Results

Here, oceanic and atmospheric response to the expansion of the full AIS (Δ_{glac}) will be the primary focus (i.e. FULL – NO), discussed in terms of temperature, atmospheric and ocean circulation, and meridional heat flux changes. The discussion of mechanisms follows in Section 4a.

Annual mean global surface air temperature (SAT) Δ_{glac} response is dominated by the cooling of up to 30 °C over the Antarctic continent in both stages, as shown in Figures 3a and 3b. The annual mean SST Δ_{glac} response varies substantially between the stages. The Priabonian shows a large area of warming of up to 6 °C over the Pacific sector of the SO, while there is cooling of up to 1.5 °C in the North Atlantic, NW Pacific and Bellingshausen Sea (Figure 3c). In contrast, the Rupelian shows more subtle variations and is more zonally heterogeneous in the Southern Hemisphere (SH), as shown in Figure 3d. Cooling occurs in much of the SH, particularly in the Indian Ocean sector of the SO by ~2 °C, while warming of up to 1.5 °C occurs in the South Pacific sector of the SO and some localised coastal areas by >3 °C. There is also year round cooling of ~6 °C in the North Atlantic. In both stages there is seasonality in the SST Δ_{glac} response, with warming being stronger during the winter (JJA) and cooling being stronger in the summer (DJF) as shown in Supplementary Figure 2. The only Δ_{glac} change in average annual sea ice concentration in either stage is a partial retreat of the sea ice in the Ross Sea during the Priabonian (figure not shown).

Annual mean mid-atmospheric pressure (*P*; expressed as the 500 hPa geopotential height) Δ_{glac} response is shown for both stages in Figures 4a and 4b. *P* decreases significantly over Antarctica and the SO and increases in southern mid-latitudes between 40-60 °S, increasing the *P* gradient at 60 °S. Changes are more pronounced for the Rupelian than the Priabonian. This response is also seasonally dominated, mostly occurring during the summer with only slight decreases in *P* over the Ross Sea edge of East Antarctica and some increases over the South Pacific and SO during winter (figure not shown). The changes in *P* result in Δ_{glac} changes in zonal winds, as shown in Figure 4c (see also Supplementary Figure 3 for annual mean wind vectors before and after glaciation). The largest changes in wind field are off the AIS due to the initiation of katabatic winds and these are persistent throughout the year. Elsewhere, changes in winds are generally geostrophic in nature, aligning with changes in the pressure gradient contours. Over the Pacific sector of the SO at 60 °S, the increased summer pressure gradient leads to strengthening and a poleward shift in the geostrophic westerlies in both stages.

Annual mean ocean zonal flow through the TS and DP for each stage and ice sheet configuration is listed in Table 2, and the depth integrated stream functions for the principle experiments (PriNO, PriFULL, RupNO, RupFULL) shown in Figure 5. There are clear differences in the ocean circulation patterns between the stages, regardless of ice sheet state. The Pacific at this time is a basin with four gateways: the DP, the TS, the Indonesian Seaway (IS) and the Panama Seaway (PS). During the Priabonian, the western gateways (TS and IS) make up the majority (68-77%) of the flow through the Pacific, whereas during the Rupelian, the southern gateways (TS and DP) represent the majority (76-

86%) of the total flow. Large gyre systems dominate the Indian, South Pacific and SO during the Priabonian. During PriNO, there is a huge Ross Sea gyre extending to ~35 °S and along the entire Antarctic coastline between the TS and DP. With the addition of the ice in PriFULL the Ross Sea gyre shrinks considerably, reaching ~45 °S and contracting westwards, no longer influencing the Bellingshausen Sea. Simultaneously, flow in the South Pacific and Indian Ocean gyres (and flow between them) strengthen. In the Rupelian, flow through the SO is zonal, dominated by a proto-ACC. Addition of the ice sheet strengthens this proto-ACC but has limited impact on the rest of the global ocean. Total flow through all Pacific gateways increases by 97% during the Priabonian but only 27% during the Rupelian in response to Δ_{glac}.

Table 2: Annual mean ocean transport through Pacific Ocean gateways for each simulation.

Simulation	Tasman Seaway through flow (Sv)	Drake Passage through flow (Sv)	Total flow through Pacific gateways (Sv)
PriNO	12.0	3.6	31.2
PriEAIS	19.8	9.2	58.0
PriFULL	21.1	9.6	61.5
RupNO	52.6	46.2	130.1
RupEAIS	71.3	64.5	159.0
RupFULL	75.2	68.0	165.8

Mixed layer depth (MLD) in the SO and North Atlantic for the four principle experiments is shown in Figure 6. There are increases of 200-1000 m in the Ross Sea for both stages and increases along the Atlantic and Indian Ocean sectors of the East Antarctic coastline by up to 1000 m in the Priabonian and 500 m in the Rupelian. There are decreases in the Weddell Sea of the Priabonian (up to 670 m) but increases in the region during the Rupelian (up to 600 m). There is a decrease in MLD in the North Atlantic in both stages. The increase in the Ross Sea MLD during the Priabonian is important, as PriNO has a very shallow MLD of <100 m, which increases up to 1000 m in PriFULL. Additionally, increased surface winds at 60 °S result in seasonal Δ_{glac} changes in the wind driven mixing in the SO, with increased upwelling to the south and increased downwelling to the north of the peak wind strength and current change. This causes a summer seasonal deepening of the MLD throughout the SO by up to 25 m (figure not shown), but this is small compared to the coastal increases previously mentioned. The global meridional overturning stream function is not shown due to the insufficient spin-up time for the deep ocean.

The meridional heat flux has the same general form for all ice sheet configurations (and stages), shown by the example of RupNO in Figure 7a. The oceanic and total heat fluxes increase southwards at all latitudes for both stages in response to Δ_{glac}, as shown in Figures 6b and 6c. The largest increases in the total southward heat flux (0.4 PW in the Priabonian; 0.3 PW in the Rupelian) occur in the SO at 65 °S, as a result of strong oceanic and atmospheric components at this latitude. The maximum increases in oceanic southward heat flux (0.4 PW in the Priabonian at ~40 °S; 0.2 PW in the Rupelian at ~60 °S) are similar in magnitude to those found in previous studies (e.g. Huber & Nof, 2006; Goldner *et al*., 2014). Changes due to gateway opening (i.e. the RupNO – PriNO; Figure 6d) show little net change in the SH total southward heat flux, with the (northwards) atmospheric component mostly balancing the (southwards) oceanic component.

4. Discussion

a) Mechanisms

Due to the complexity of GCMs, and in particular the feedbacks which act between many aspects of the system, diagnosing the mechanisms behind changes seen in the model in response to a change in boundary conditions is challenging. The only way to confidently assess mechanisms is to carry out sensitivity studies in which particular aspects of the system are kept constant, and/or feedback loops are cut. However, due to the computational cost of additional simulations, this is rarely carried out. Here, the mechanisms behind the observed responses will be discussed qualitatively. We aim to provide plausible mechanistic explanations for the changes seen in both stages, but without additional sensitivity studies these mechanisms remain somewhat speculative.

Two fundamental factors of Antarctic glaciation affect climate: 1) the increased surface albedo over the continent, reducing the solar radiation absorbed at the surface, and 2) the increased height of the new ice sheet topography, changing the reference height and modifying atmospheric pressure and circulation. The combined effect of these two factors causes the dramatic SAT cooling over Antarctica (Figure 3). The gravitational potential of this cold air initiates katabatic winds off the ice sheet (e.g. Parish & Waight, 1987). The outflow of the katabatic winds enhances polar circulation over Antarctica, and so between 60-80 °S air is rising to replace that flowing off the AIS leading to reduced *P* (Figure 4). It would be expected that cooling air over the AIS would lead to sinking and be associated with increasing *P* (similar to Goldner *et al*., 2014). However, the strong temperature seasonality of HadCM3L over Antarctica (Gasson *et al*., 2013) negates this pressure effect with large decreases in summer *P*. It should be noted, however, in terms of mean sea level pressure, *P* is found to increase over Antarctica (figure not shown; similar to Goldner *et al*., 2014). This is subject to interpolation that may be unrealistic when adding a thick AIS.

Regardless of the mechanism of *P* change over the AIS, the Δ_{glac} decrease over the SO is expected and results in an increased north-south pressure gradient at the polar front, ~60 °S. This causes increases in westerly winds over the Pacific sector of the SO (Figure 4c) that result in slight changes in the wind-driven eastward flow (Allison *et al.*, 2010). The change in zonal wind stress over the SO leads to some increased wind driven upwelling south of 60 °S and downwelling north of 60 °S (figure not shown). Some of this wind driven overturning change would be expected to be balanced by an increased eddy field, however, the relatively coarse model resolution means that these eddies are not resolved (Abernathey *et al*., 2011; Munday *et al*., 2015).

By comparing the Δ_{glac} SST response with the change in SST observed between the stages with the same ice sheet states (Supplementary Figure 4), it is possible to identify PriNO as having an anomalously cold Ross Sea and South Pacific sector. This sensitive stratified ocean state is associated with a lack of deep-water formation in the region, indicated by the very shallow MLD (Figure 6a). Deep-water formation draws water from lower latitudes, releasing heat as it sinks. The interconnectivity of the causes and changes associated with deep-water formation make untangling these results particularly challenging, but a potential explanation of why this process is absent during PriNO is offered here.

During the Priabonian, constricted ocean gateways do not allow a strong barotropic circumpolar current to form around Antarctica, with eastward flowing water in the Pacific sector being part of larger South Pacific or Ross Sea gyre circulations (Figures 5a and 5b). The sluggish zonal circulation prior to glaciation allows the Ross Sea gyre to expand both northwards and eastwards across the width

of the Pacific sector of the SO (similar to Sijp *et al*., 2011 with a closed TS). As a result, water is transferred to high latitudes along the eastern boundary of the Pacific and returns westwards along the Antarctic coastline, and is very cold upon reaching the Ross Sea. Combined with the lack of deep-water formation and a sea ice albedo feedback, this causes the region to be anomalously cold compared to the other simulations. Deep-water formation in the polar regions is strongly affected by salinity (Assmann & Timmermann, 2005), so despite the low Ross Sea SST in PriNO water density and deep-water formation are suppressed by low salinities (Supplementary Figure 5a). With the addition of the AIS (or expansion of the gateways), the salinity in the Ross Sea increases (Supplementary Figure 5b), initiating sinking. This salinity change could be the result of changes in sea ice formation, changes in net evaporation and precipitation (*E*-*P*) and/or changes in ocean circulation.

Changes in sea ice formation are ruled out as being an important driver of the Ross Sea Δ_{glac} salinity response, because sea ice extent reduces with the inclusion of the ice sheet, which will result in less brine rejection. Sea ice causes a seasonal increase in salinities but this effect diminishes once the ice sheet forms. The South Pacific and SO experience net precipitation (*P*>*E*) in all simulations, contributing to the low salinities found there. In the SO the highest salinities are close to the TS and decrease with distance east (Supplementary Figure 5). The *E*-*P* Δ_{glac} response shows an increase in evaporation over the Ross Sea of the Priabonian, but there is still net precipitation over the region. This may not be the driver of change but will act as a positive feedback with deep-water formation (whereby enhanced evaporation increases salinity, potentially increasing deep-water formation, which in turn releases heat and further enhances evaporation). Pacific sector salinity shows a strong correlation with flow through the TS from the high salinity Indian Ocean. It is plausible that the low salinity in PriNO is due to the greatly reduced flow through the TS. Once flow is increased, either by opening the gateway or adding the ice sheet, high salinity water penetrates into the Ross Sea, initiating deep-water formation.

A combination of the latter two processes is likely to have brought about the change in the Ross Sea salinity, with advection of water through the TS potentially triggering and enhanced *E* consolidating the increase (Sijp *et al*., 2011). Deep-water formation then enhances meridional transport of water, causing the large Ross Sea gyre to contract westwards away from the Bellingshausen Sea. As a result, the Bellingshausen Sea coast cools (less meridional transport to the region) and the Ross Sea warms. The warming is strong and extensive in contrast to the results of Sijp *et al*. (2011), who compared a fully open and closed TS but with no change in ice sheet. Further feedbacks may have contributed to this strong response: firstly with the collapse of sea ice and associated albedo effect enhancing the temperature anomaly in the region; secondly with the smaller Ross Sea gyre reducing the transport time of water within the gyre, reducing the freshening effect of the negative net *E*-*P* in the region; and thirdly with steepening of the isopycnals in the SO resulting in a stronger zonal depth integrated stream function through thermal wind.

The Rupelian SST Δ_{glac} response is not as strong as the Priabonian, but there are still some clear spatial and seasonal patterns. The warming and cooling responses can be explained by separate mechanisms. The summer SST cooling over the Indian Ocean sector of the SO appears to be a direct result of glaciation through atmospheric cooling and katabatic winds. The proximity of the Indian Ocean sector to the EAIS, where there is Δ_{glac} cooling of >30 °C and katabatic winds to transfer this extremely cold air over the SO, affects the summer SST. The Δ_{glac} change in southward heat flux (Figure 7c) shows a global increase in the oceanic component, suggesting that the cooling has a local source and is not the result of changes in ocean circulation (i.e. reduced southward heat flux). Future work will aim to confirm this by comparing results to simulations with a slab ocean with a fixed

ocean heat flux (which we hypothesise to show the same signal). In the winter, the Δ_{glac} warming response found in the South Pacific sector of the SO is caused by circulation changes. Stronger westerlies and seasonally persistent katabatic winds intensify the Ross Sea gyre (shown by the sharper 'kink' in the depth integrated stream lines in Figure 5d and the surface currents in Supplementary Figure 5d), transferring waters meridionally and bringing heat southwards. The signal is not as clear during the summer, however, because the increased westerly winds at 60 °S transfer colder water from the Indian Ocean sector to the Pacific sector of the SO and Ross Sea, overprinting the signal. Some stronger warming occurs along coastlines where there is enhanced deep-water formation, shown by the increases in MLD between Figures 6c and 6d.

It should be noted that the responses and mechanisms outlined here are also consistent for glaciation of only East Antarctica, with the main area of Ross Sea warming still present during the Priabonian but having a slightly lower magnitude (exhibiting maximum warming values of ~4.5 °C; figure not shown). There are only subtle variations in the Weddell Sea MLD and SST responses to East Antarctic glaciation compared to those discussed here, showing the effect of the WAIS is small and localised.

b) Implications

These results would suggest that prior to an established proto-ACC (or sufficient TS opening) there is a negative feedback on AIS growth, in which increases in Antarctic ice volume lead to large increases in SST in the Pacific SO, potentially inhibiting further Antarctic ice growth. If this were the case, it may have and contributed to the temporality of ephemeral ice sheets during the Eocene (Miller *et al*., 2008). This feedback wanes once the TS and DP widen and the ACC becomes stronger, with cooler summer SO temperatures, particularly in the Indian Ocean sector. There is also a potential mild positive feedback with winter warming in the coastal SO, which may enhance evaporation and Antarctic ice growth. However, there is evidence for a limited effect of SST changes on the interior of the Antarctic continent within models (Huber & Nof, 2006)

Additionally, the unglaciated Priabonian results are inconsistent with some of the (albeit limited) proxy datasets available. Douglas *et al*. (2014) find a zonal gradient in SST proxies between the warmer southwest Pacific and the cooler south Atlantic of 7 °C during the middle-to-late Eocene. A similar temperature gradient is found here for the Rupelian, but not for the Priabonian (see Supplementary Figure 6). During the Rupelian, the gradient is greater when Antarctica is unglaciated (4 °C), reducing slightly with glaciation (3 °C) due to the cooling and transfer of Indian Ocean sector waters reducing the peak temperatures found in Pacific sector. It should be noted the absolute values are ~15 °C cooler than the simulations and proxy reconstructions of Douglas *et al*. due to the different atmospheric CO_2 levels used (their simulations used 2,400 and 1,600 ppm, representative of the mid-to-late Eocene). We suggest, therefore, the key implication of these results is that subtle changes in palaeogeography and model setup can result in substantially different regional climate responses: potentially of great importance when interpreting model results. Hence, it is not surprising that the results differ from those of Goldner *et al*. (2014) and Knorr & Lohmann (2014).

This conclusion is further corroborated by comparing the zonal flow Δ_{glac} response for the Rupelian with the results of Hill *et al.* (2013). In our study, adding the AIS in the Rupelian increases zonal flow by >20 Sv (10^6 m^3 s^{-1}) whereas Hill *et al*. found it reduced flow through the DP and TS by 2 and 10 Sv respectively. Although their simulations were also carried out using the same model (HadCM3L) and atmospheric CO_2 levels, their spin-up procedure, model setup and palaeogeographic

reconstructions were different, highlighting how experimental design can impact results, even using the same model.

A number of additional experiments were carried out with the same spin-up procedures as those discussed here. One of these was an ice-free Priabonian simulation with four times pre-industrial CO_2 levels (more physically realistic for the late Eocene; Pearson *et al*., 2009; Pagani *et al*., 2011). This experiment also showed a very cold Ross Sea with no deep-water formation, so while we note this result is likely to be model dependent, it is robust to a change in CO_2 concentration. Another set of simulations was carried out for the Chattian stage (~28-23 Ma) that follows the Rupelian (~34-28 Ma). In this stage there was further widening of the TS and DP by another grid cell in the model, and the same ice sheet and ice-free configurations were used. With this additional opening of the southern gateways flow approximately doubles compared to the Rupelian, and with the addition of the AIS there is an established ACC and flow through the DP of 103.5 Sv (a similar order of magnitude to present day measurements of ~130 Sv; Meredith *et al.*, 2004). This would support studies suggesting the ACC strengthened in the mid-to-late Oligocene (Pfuhl & McCave, 2005; Lyle *et al*., 2007). It is also worth noting the zonal flow through the DP and TS is once again different to the results of Hill *et al.* (2013), being 10-20 Sv higher in our study.

All stages (including the Chattian) show that enhanced zonal ocean circulation due to Antarctic glaciation and gateway opening causes increased poleward heat transport in the Southern Hemisphere, contrary to traditional theory (e.g. Gill & Bryan, 1971; Kennett, 1977; England, 1993) but similar to the results of Goldner *et al*. (2014). These results suggest that the enhanced circulation does not act as a barrier to inhibit poleward heat transport. As noted previously, these increases are similar to those found in previous studies (Huber & Nof, 2006; Goldner *et al*., 2014), however, it remains to be seen if it is great enough to have a significant effect on Antarctic climate (Huber & Nof, 2006).

5. Conclusions

This study identified the climatic and oceanic response to glaciation in the HadCM3L model for two geological stages on either side of the EOT. The climatic response to glaciation varied significantly between the two stages, due to a complex network of feedbacks acting to cool the Ross Sea during the unglaciated Priabonian simulation. The sensitive, cold ocean state in this simulation is easily destabilised with the onset of deep-water formation in response to either Antarctic glaciation or gateway opening. This response is likely to be very model dependent (it does not match with the limited proxy data available for the region for example), but it highlights how, through multiple feedbacks, subtle changes in palaeogeography and model setup can produce very different modelled climatic responses to Antarctic glaciation.

Future research can expand in multiple directions. Initial work could carry out a slab ocean model run for the Rupelian to affirm the conclusions about Indian Ocean cooling being due to the proximity with the AIS. Running similar experiments with different coupled climate models will be essential in assessing if this sensitive behaviour is a feature of other models, or if this is specific to HadCM3L. Further work will also include more detailed comparison of the modelled response to the geological record. Finally, using these high-resolution palaeogeographic reconstructions, it would be interesting to carry out transient simulations under changing CO_2 forcing with a coupled ice sheet model (similar to those of DeConto & Pollard, 2003 and Ladant *et al*., 2014) to model glacial inception and examine

if regional sensitivity exists in this case also, and to properly explore the feedbacks between Antarctica and global climate.

References

Abernathey, R., Marshall, J. & Ferreira, D. 2011. The Dependence of Southern Ocean Meridional Overturning on Wind Stress. *Journal of Physical Oceanography*, 41, pp. 2261-2278, DOI: 10.1175/JPO-D-11-023.1.

Allison, L.C., Johnson, H.L., Marshall, D.P. & Munday, D.R. 2010. Where do winds drive the Antarctic Circumpolar Current? *Geophysical Research Letters*, 37, L12605, DOI: 10.1029/2010GL043355.

Assmann, K.M. & Timmermann, R. 2005. Variability of deep water formation in the Ross Sea. *Ocean Dynamics*, 55, pp. 68-87, DOI: 10.1007/s10236-004-0106-7.

Barker, P.F. & Thomas, E. 2004. Origin, signature and palaeoclimatic influence of the Antarctic Circumpolar Current. *Earth-Science Reviews*, 66, pp. 143-162, DOI: 10.1016/j.earscirev.2003.10.003.

Barker, P.F., Filippelli, G.M., Florindo, F., Martin, E.E. & Scher, H.D. 2007. Onset and role of the Antarctic Circumpolar Current. *Deep Sea Research II*, 54, pp. 2388-2398, DOI: 10.1016/j.dsr2.2007.07.028.

Bohaty, S.M., Zachos, J.C. & Delaney, M.L. 2012. Foraminiferal Mg/Ca evidence for Southern Ocean cooling across the Eocene-Oligocene transition. *Earth and Planetary Science Letters*, 317-318, pp. 251-261, DOI: 10.1016/j.epsl.2011.11.037.

Cox, P. M., 2001: Description of the TRIFFID dynamic global vegetation model. Tech. Note 24, Hadley Centre, Met Office, 16 pp.

Cox, P.M., Betts, R.A., Jones, C.D., Spall, S.A. & Totterdell, I.J., 2001. Modelling vegetation and the carbon cycle as interactive elements of the climate system, in *Meteorology at the Millennium*, edited by Pearce, R., pp. 259-279, Academic Press, San Diego, California.

Coxall, H.K., Wilson, P.A., Pälike, H., Lear, C.H. & Backman, J., 2005. Rapid stepwise onset of Antarctic glaciation and deeper calcite compensation in the Pacific Ocean. *Nature*, 433, pp. 53-57, DOI: 10.1038/nature03135.

DeConto, R. M. & Pollard, D., 2003. Rapid Cenozoic glaciation of Antarctica induced by declining atmospheric CO_2. *Nature*, 421, pp. 245-249.

Douglas, P.M.J., Affek, H.P., Ivany, L.C., Houben, A.J.P., Sijp, W.P., Sluijs, A., Schouten, S. & Pagani, M., 2014. Pronounced zonal heterogeneity in Eocene southern high-latitude sea surface temperatures. *PNAS*, 111, 18, pp. 6582-6587, DOI: 10.1073/pnas.1321441111.

England, M.H., 1993. Representing the Global-Scale Water Masses in Ocean General Circulation Models. *Journal of Physical Oceanography*, 23, pp. 1523-1552, DOI: http://dx.doi.org/10.1175/1520-0485(1993)023<1523:RTGSWM>2.0.CO;2

Foster, G.L. & Rohling, E.J. 2013. Relationship between sea levels and climate forcing by CO_2 on geological timescales. *PNAS*, 110, 4, pp. 1209-1214, DOI: 10.1073/pnas.1216073110.

Gasson, E., Lunt, D.J., DeConto, R., Goldner, A., Heinemann, M., Huber, M., Legrande, A.N., Pollard, D., Sagoo, N., Siddall, M. & Winguth, A., 2013. Uncertainties in the modelled CO_2 threshold for Antarctic glaciation. *Climate of the Past Discussions*, 9, pp. 5701-5745, DOI: 10.5194/cpd-9-5701-2013.

Gill, A.E. & Bryan, K., 1971. Effects of geometry on the circulation of a three-dimensional southern-hemisphere ocean model. *Deep Sea Research*, 18, 7, pp. 685-721.

Goldner, A., Huber, M. & Caballero, R., 2013. Does Antarctic glaciation cool the world? *Climate of the Past*, 9, pp. 173-189, DOI: 10.5194/cp-9-173-2013.

Goldner, A., Herold, N. & Huber, M., 2014. Atlantic glaciation caused ocean circulation changes at the Eocene-Oligocene transition. *Nature*, 511, pp. 574-577, DOI: 10.1038/nature13597.

Gordon, C., Cooper, C., Senior, C.A., Banks, H., Gregory, J.M., Johns, T.C., Mitchell, J.F.B. & Wood, R.A., 2000. The simulation of SST, sea-ice extents and ocean heat transports in a version of the Hadley Centre coupled model without flux adjustments. *Climate Dynamics*, 16, pp. 147-168.

Hill, D.J., Haywood, A.M., Valdes, P.J., Francis, J.E., Lunt, D.J., Wade, B.S. & Bowman, V.C. 2013. Paleogeographic controls on the onset of the Antarctic circumpolar current. *Geophysical Research Letters*, 40, pp. 5199-5204, DOI: 10.1002/grl.50941.

Huber, M., Brinkhuis, H., Stickley, C.E., Doos, K., Sluijs, A., Warnaar, J., Schellenberg, S.A. & Williams, G.L., 2004. Eocene circulation of the Southern Ocean: Was Antarctica kept warm by subtropical waters? *Paleoceanography*, 19, PA4026, doi: 10.1029/2004PA001014.

Huber, M. & Nof, D., 2006. The ocean circulation in the southern hemisphere and its climatic impacts in the Eocene. *Palaeogeography, Palaeoclimatology, Palaeoecology*, 231, pp. 9-28.

Inglis, G.N., Farnsworth, A., Lunt, D.J., Foster, G.L., Hollis, C.J., Pagani, M., Jardine, P.E., Pearson, P.N., Markwick, P.J., Raynman, L., Galsworthy, A.M.J. & Pancost, R.D. Descent towards the Icehouse: Eocene sea surface cooling inferred from GDGT distributions, in press, Paleoceanography.

Jones, C., 2003. A fast ocean GCM without flux adjustments. *Journal of Atmospheric and Oceanic Technology*, 20, pp. 1857-1868.

Katz, M.E., Miller, K.G., Wright, J.D., Wade, B.S., Browning, J.V., Cramer, B.S. & Rosenthal, Y. 2008. Stepwise transition from the Eocene greenhouse to the Oligocene icehouse. *Nature Geoscience*, 1, 329-334, DOI: 10.1038/ngeo179.

Kennett, J.P., 1977. Cenozoic evolution of Antarctic glaciation, circum Antarctic ocean, and their impact on global paleoceanography. *Journal of Geophysical Research*, 82, pp. 3843-3860, DOI: 10.1029/JC082i027p03843.

Kennett, J.P., & Shackleton, N.J., 1976. Oxygen isotopic evidence for the development of the psychrosphere 38 Myr ago. *Nature*, 260, pp. 513-515, DOI: 10.1038/260513a0.

Knorr, G. & Lohmann, G., 2014. Climate warming during Antarctic ice sheet expansion at the Middle Miocene transition. *Nature Geoscience*, 7, pp. 376-381, DOI: 10.1038/ngeo2119.

Ladant, J.B., Donnadieu, Y., Lefebvre, V. & Dumas, C., 2014. The respective role of atmospheric carbon dioxide and orbital parameters on ice sheet evolution at the Eocene-Oligocene transition. *Paleoceanography*, DOI: 10.1002/2013PA002593.

Lear, C.H., Rosenthal, Y., Coxall, H.K. & Wilson, P.A., 2004. Late Eocene to early Miocene ice-sheet dynamics and the global carbon cycle. *Paleoceanography*, 19, PA4015, DOI: 10.1029/2004PA001039.

Lear, C.H., Bailey, T.R., Pearson, P.N., Coxall, H.K., & Rosenthal, Y., 2008. Cooling and ice growth across the Eocene–Oligocene transition. *Geology*, 36, pp. 251-254, DOI: 10.1130/G24584A.1.

Lear, C.H., Mawbey, E.M., & Rosenthal, Y., 2010. Cenozoic benthic foraminiferal Mg/Ca and Li/Ca records: Toward unlocking temperatures and saturation states. *Paleoceanography*, 25, PA4215, DOI: 10.1029/2009PA001880.

Lefebvre, V., Donnadieu, Y., Sepulchre, P., Swingedouw, D. & Zhang, Z.S., 2012. Deciphering the role of southern gateways and carbon dioxide on the onset of the Antarctic Circumpolar Current. *Paleoceanography*, 27, PA4201, DOI: 10.1029/2012PA002345.

Liu, Z., Pagani, M., Zinniker, D., DeConto, R., Huber, M., Brinkhuis, H., Shah, S.R., Leckie, R.M., & Pearson, A., 2009. Global cooling during the Eocene–Oligocene climate transition. *Science*, 323, pp. 1187-1190, DOI: 10.1126/science.1166368.

Lunt, D.J., Ross, I., Hopley, P.J., Valdes, P.J. (2007) Modelling Late Oligocene C4 grasses and climate. Palaeogeography, Palaeoclimatology, Palaeoecology, 251, 239-253.

Lyle, M., Gibbs, S., Moore, T.C. & Rea, D.K., 2007. Late Oligocene initiation of the Antarctic Circumpolar Current: Evidence from the South Pacific. *Geology*, 35, pp.691-694.

Marchitto T. M., Curry, W. B., Lynch-Stieglitz, J., Bryan, S. P., Cobb, K.M. & Lund, D. C., 2014. Improved oxygen isotope temperature calibrations for cosmopolitan benthic foraminifera, *Geochimica et Cosmochimica Acta* 130 1–11.

Markwick, P.J., 2007. The palaeogeographic and palaeoclimatic significance of climate proxies for data-model comparisons, in *Deep-time perspectives on climate change: Marrying the signal from computer models and biological proxies*, edited by Williams, M. et al. pp. 251-312, Micropalaeontological Society, Special Publications, The Geological Society, London.

Meredith, M.P., Woodworth, P.L., Hughes, C.W. & Stepanov, V., 2004. Changes in the ocean transport through the Drake Passage during the 1980s and 1990s, forced by changes in Southern Annular mode. *Geophysical Research Letters*, 31, L21305, DOI: 10.1029/2004GL021169.

Miller, K.G., Wright, J., Katz, M., Browning, J., Cramer, B., Wade, B.S. & Mizintseva, S., 2008. A view of Antarctic ice-sheet evolution from sea-level and deep-sea isotope changes during the Late Cretaceous-Cenozoic, in *Antarctica: A Keystone in a Changing World*, pp. 55-70, Natl. Acad., Washington D.C.

Munday, D.R., Johnson, H.L. & Marshall, D.P., 2015. The role of ocean gateways in the dynamics and sensitivity to wind stress of the early Antarctic Circumpolar Current. *Paleoceanography*, 30, doi: 10.1002/2014PA002675.

Pagani, M., Huber, M., Liu, Z., Bohaty, S.M., Henderiks, J., Sijp, W., Krishnan, R. & DeConto, R.M. 2011. The Role of Carbon Dioxide During thr Onset of Antarctic Glaciation. *Science*, 334, pp. 1261-1264, DOI: 10.1126/science.1203909.

Parish, T.R. & Waight, K.T., 1987. The Forcing of Antarctic Katabatic Winds. *Monthly Weather Review*, 115, pp. 2214-2226.

Pearson, P.N., McMillan, I.K., Wade, B.S., Dunkley Jones, T., Coxall, H.K., Bown, P.R., & Lear,

C.H., 2008. Extinction and environmental change across the Eocene–Oligocene boundary in Tanzania. *Geology*, 36, pp. 179-182, DOI: 10.1130/G24308A.1.

Pearson, P.N., Foster, G.L., & Wade, B.S., 2009. Atmospheric carbon dioxide through the Eocene–Oligocene climate transition. *Nature*, 461, pp. 1110-1113, DOI: 10.1038/nature08447.

Peck, V.L., Yu, J., Kender, S. & Riesselman, C.R., 2010. Shifting ocean carbonate chemistry during the Eocene-Oligocene climate transition: Implications for deep-ocean Mg/Ca paleothermometry. *Plaeoceanography*, 25, PA4219, DOI :10.1029/2009PA001906.

Pfuhl, H.A. & McCave, I.N., 2005. Evidence for late Oligocene establishment of the Antarctic Circumpolar Current. *Earth and Planetary Science Letters*, 235, pp. 715-728, DOI: 10.1016/j.epsl.2005.04.025.

Pusz, A.E., Thunell, R.C. & Miller, K.G., 2011. Deep water temperature, carbonate ion, and ice volume changes across the Eocene-Oligocene climate transition. *Paleoceanography*, 26, PA2205, DOI: 10.1029/2010PA001950.

Sijp, W.P. & England, M.H., 2004. Effect of Drake Passage Throughflow on Global Climate. *Journal of Physical Oceanography*, 34, pp. 1254-1266.

Sijp, W.P., England, M.H. & Huber, M., 2011. Effect of deepening the Tasman Gateway on the global ocean. *Paleoceanography*, 26, PA4207, doi: 10.1029/2011PA002143.

Stickley, C.E., Brinkhuis, H., Schellenberg, S.A., Sluijs, A., Rohl, U., Fuller, M., Grauert, M., Huber, M., Warnaar, J. & Williams, G.L., 2004. Timing and nature of the deepening of the Tasmanian Gateway. *Paleoceanography*, 19, PA4027, doi: 10.1029/2004001022.

Wade, B.S., Houben, A.J.P., Quaijtaal, W., Schouten, S., Miller, K.G., Katz, M.E., Wright, J.D. & Brinkhuis, H., 2012. Multiproxy record of abrupt sea-surface cooling across the Eocene-Oligocene transition in the Gulf of Mexico. *Geology*, 40, 2, pp. 159-162, DOI:10.1130/G32577.1.

Zachos, J.C., Quinn, R.M., & Salamy, K., 1996. High resolution (104 yr) deep-sea foraminiferal stable isotope records of the Eocene–Oligocene climate transition. *Paleoceanography*, 11, pp. 251-266, DOI: 10.1029/96PA00571.

Zachos, J.C. & Kump, L.R., 2005. Carbon cycle feedbacks and the initiation of Antarctic glaciation in the earliest Oligiocene. *Global and Planetary Change*, 47, pp. 51-66, DOI: 10.1016/j.gloplacha.2005.01.001.

Zachos, J.C., Shackleton, N.J., Revenaugh, J.S., Pälike, H. & Flower, B.P., 2001. Trends, Rhythms, and Aberrations in Global Climate 65 Ma to Present. *Science*, 292, pp. 686-693, DOI: 10.1126/science.1059412.

Zachos, J.C., Dickens, G.R. & Zeebe, R.E., 2008. An early Cenozoic perspective on greenhouse warming and carbon cycle dynamics, *Nature*, 551 (7176), pp. 279-283, DOI: 10.1038/nature06588.

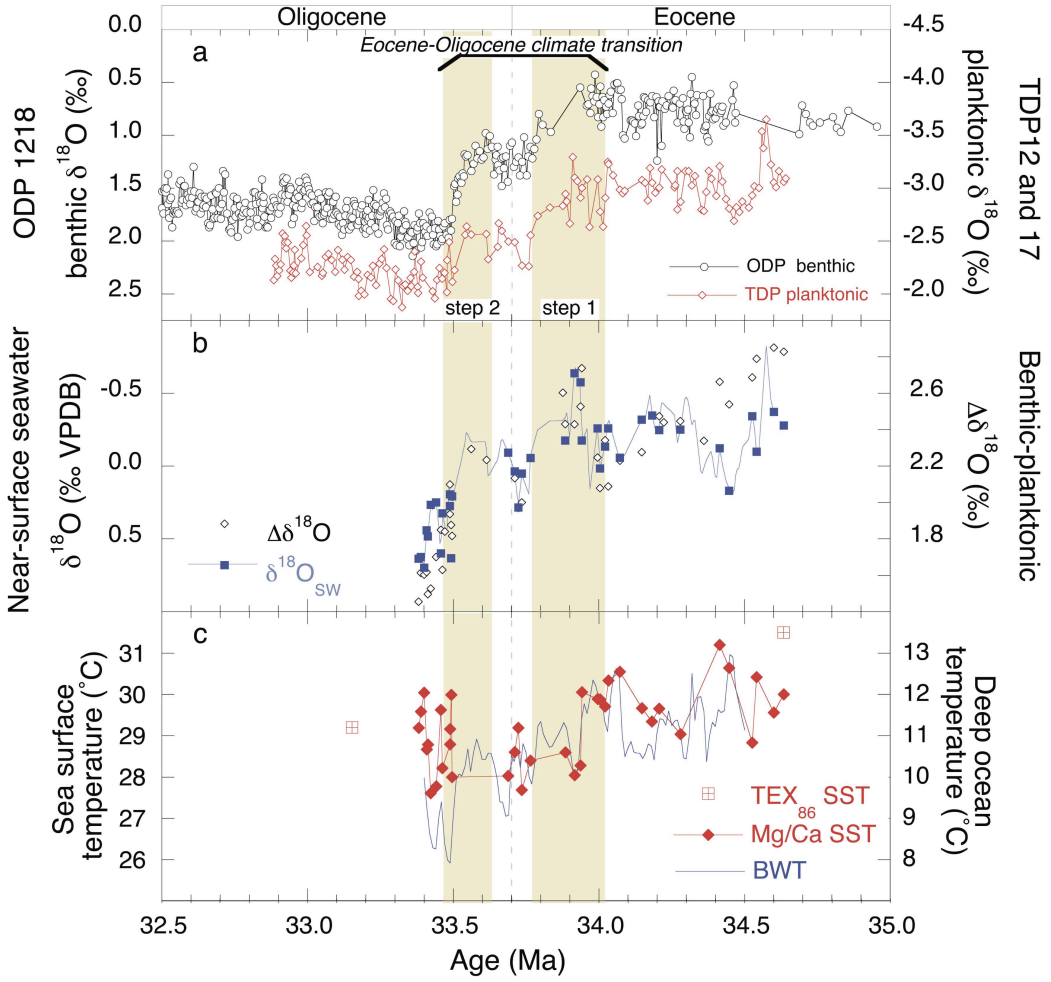

Figure 1: Multi-proxy records of climatic and palaeoceanographic change across the Eocene-Oligocene transition. Foraminiferal $\delta^{18}O$ records (a): black circles - benthic foraminiferal $\delta^{18}O$ from ODP Site 1218 (Coxall et al., 2005), red diamonds - planktonic foraminiferal $\delta^{18}O$ from TDP Sites 12 and 17 (Pearson et al., 2008). Proxy records of ice growth (b): blue line - near-surface $\delta^{18}O_{sw}$ calculated by interpolating TDP planktonic Mg/Ca and $\delta^{18}O$ records, solid blue squares – near-surface $\delta^{18}O_{sw}$ calculated using TDP planktonic Mg/Ca temperatures and interpolated TDP planktonic $\delta^{18}O$ record, open black diamonds – TDP benthic-planktonic $\delta^{18}O$ gradient, in part reflecting local water depth, calculated from *Epistomina* sp. $\delta^{18}O$ and interpolated *T. ampliapertura* $\delta^{18}O$ (Lear et al., 2008). Sea surface and deep ocean temperature (c): Red diamonds - SSTs based on TDP planktonic foraminiferal Mg/Ca (red diamonds), red hatched squares – SSTs based on TDP TEX86, blue line – deep ocean temperature calculated using the ODP Site 1218 benthic foraminiferal $\delta^{18}O$ record (Coxall et al., 2005) with the $\delta^{18}O_{sw}$ record derived from TDP sites (Lear et al., 2008) and the palaeotemperature equation of Marchitto et al., 2014. Yellow shaded bars highlight the two "steps" of the oxygen isotope shift (Coxall et al., 2005), and vertical dashed black line marks E-O boundary as defined by extinction of the Family Hantkeninidae.

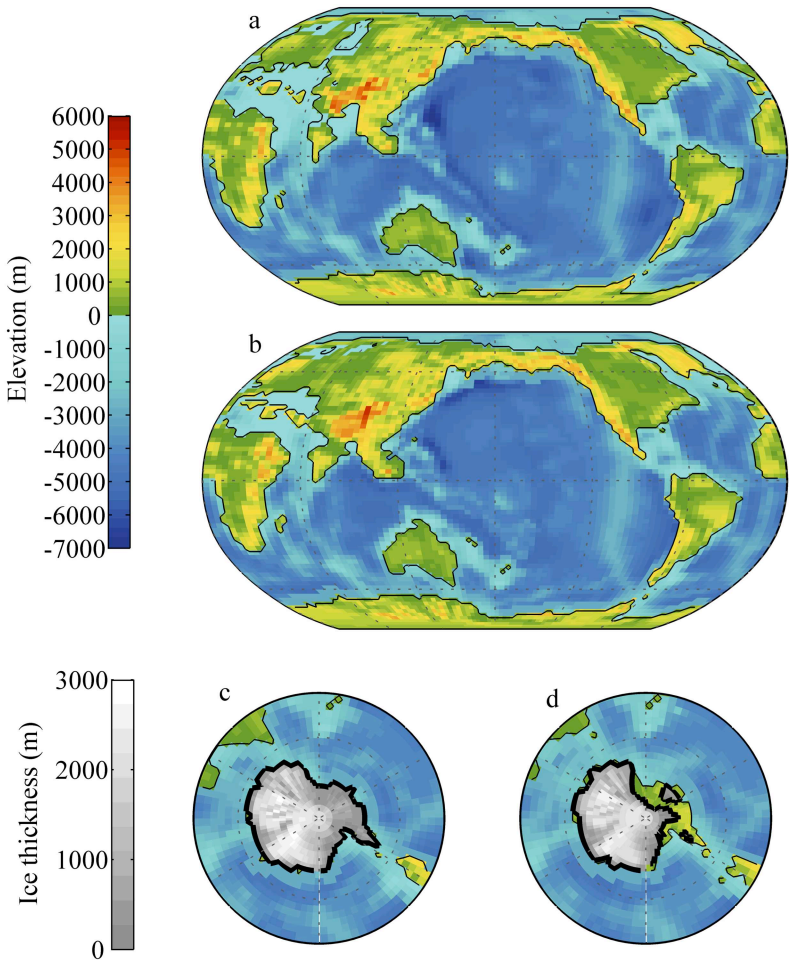

Figure 2: Palaeogeographic reconstructions of topography and bathymetry (m) for the Priabonian (a) and Rupelian (b) stages shown at model resolution. The thickness (m) and extent of the reconstructed full (c) and East Antarctic ice sheets (d) are also shown.

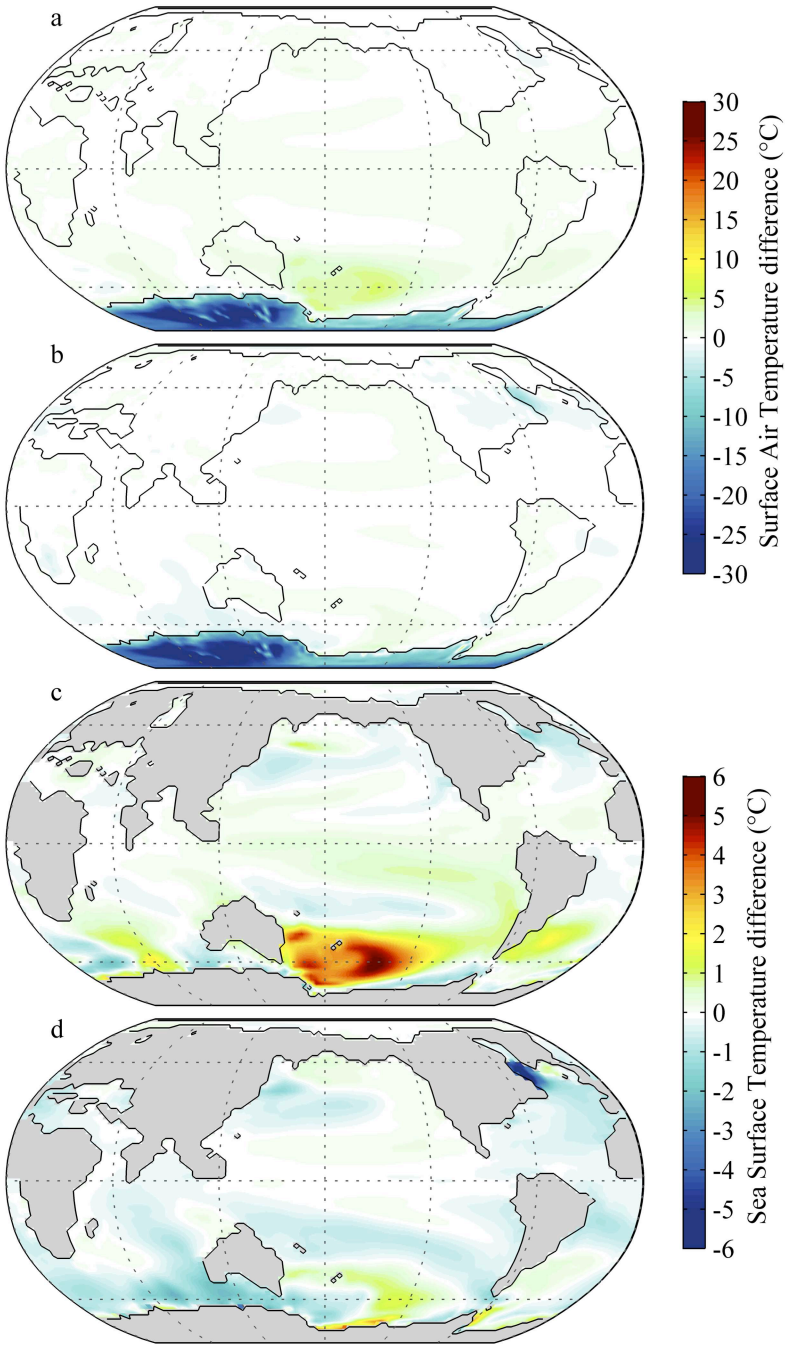

Figure 3: Annual mean surface air temperature response (°C) to Antarctic glaciation for the Priabonian (a) and Rupelian (b), and annual mean sea surface temperature response (°C) to glaciation for the Priabonian (c) and Rupelian (d).

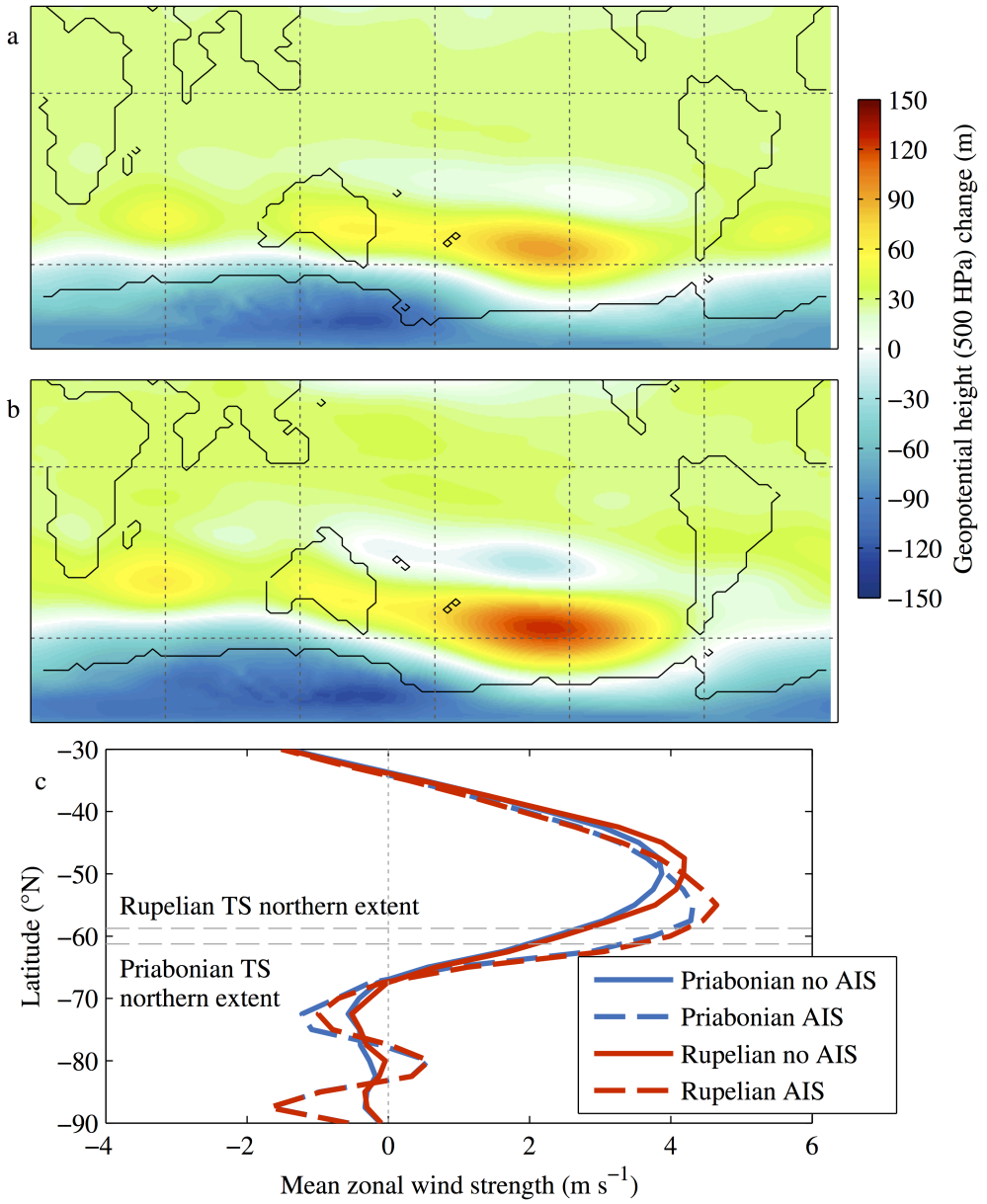

Figure 4: Changes in annual mean 500 hPa geopotential height (m) in response to Antarctic glaciation for the Priabonian (a) and Rupelian (b), and mean zonal westerly wind strength (m s^{-1}) for each stage and ice sheet configuration (c).

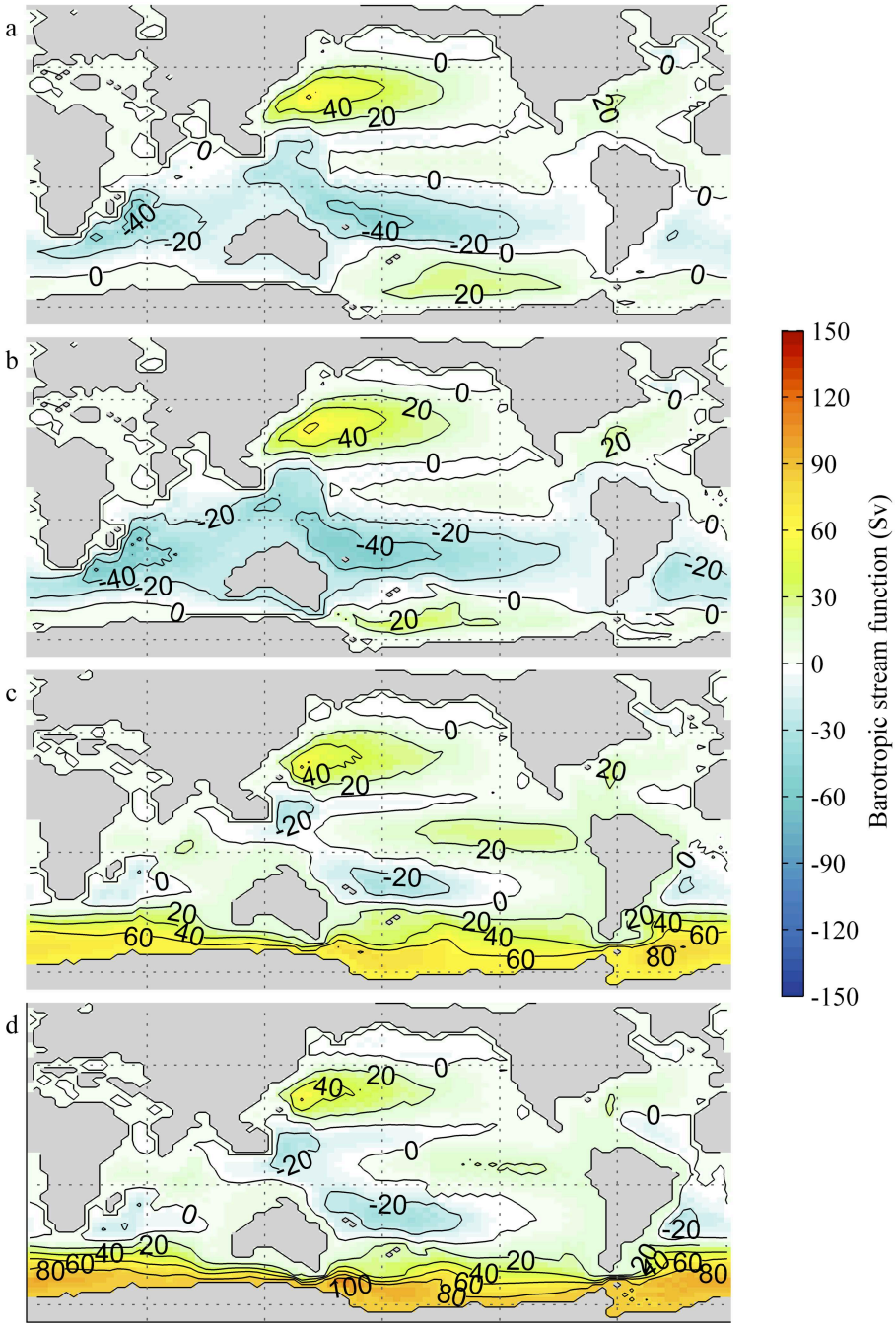

Figure 5: Annual mean barotropic stream function (Sv) for the Priabonian: unglaciated (a) and glaciated (b); and Rupelian: unglaciated (c) and glaciated (d).

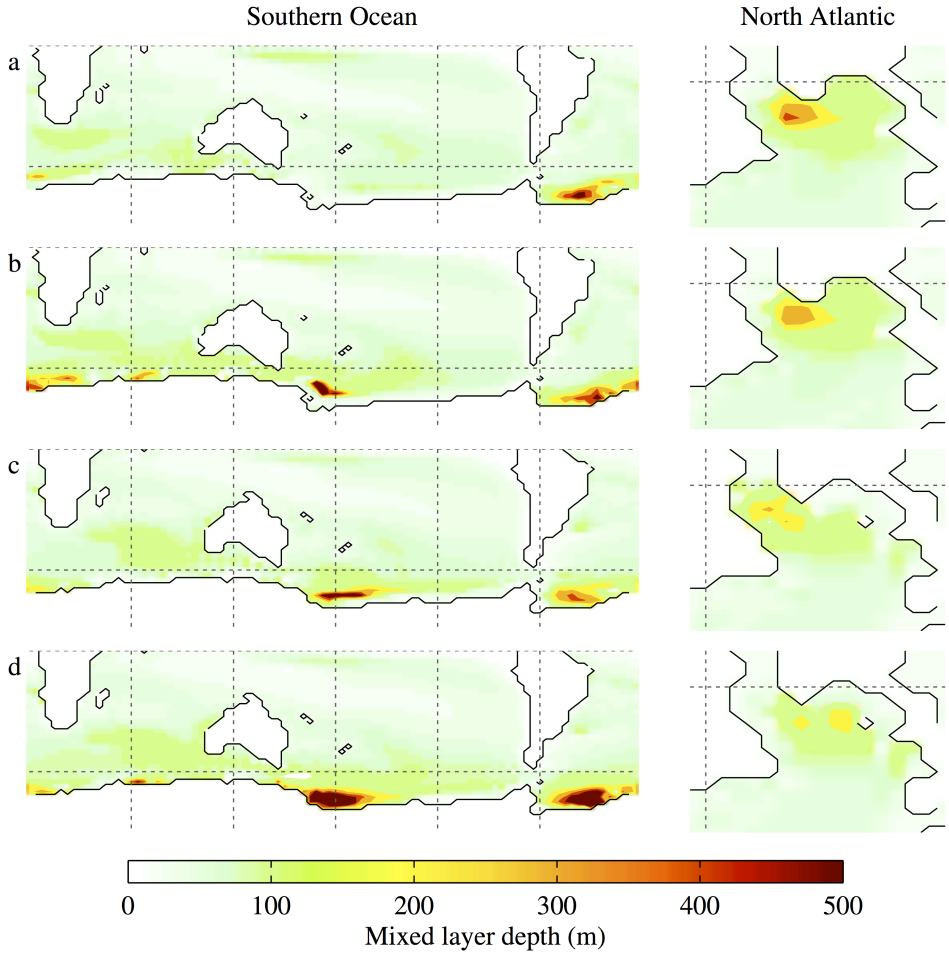

Figure 6: Annual mean mixed layer depth (m) in the Southern Ocean (left) and North Atlantic (right) for the Priabonian: unglaciated (a) and glaciated (b); and Rupelian: unglaciated (c) and glaciated (d). The mixed layer is very shallow in the North Pacific in all simulations.

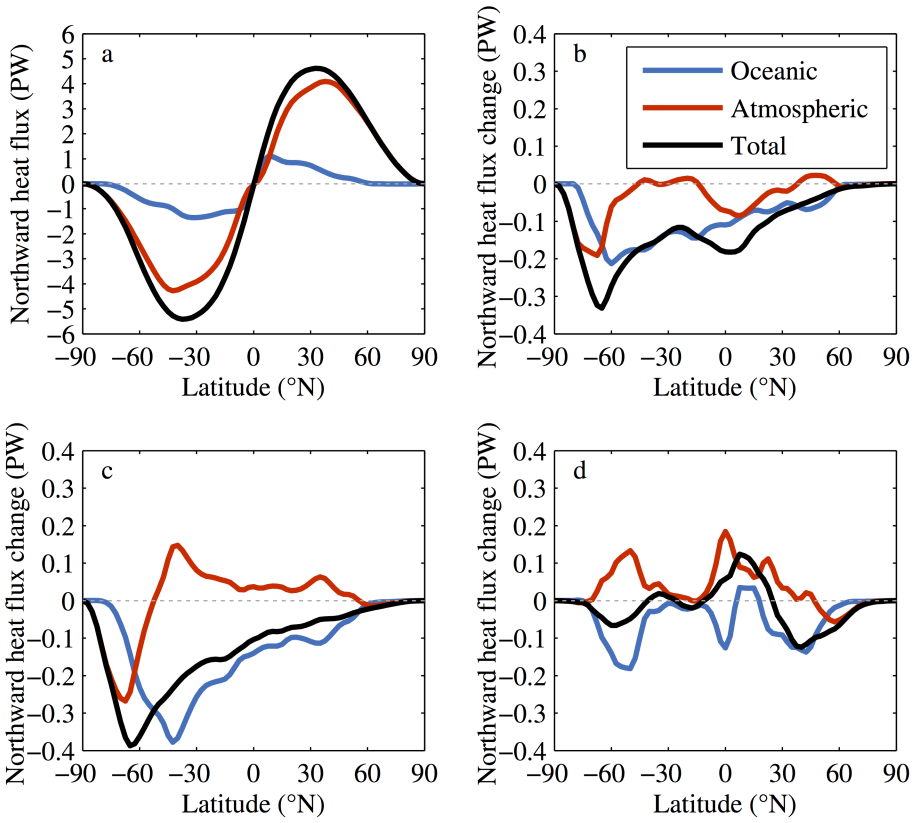

Figure 7: General form of the global meridional (northward) heat flux (PW), shown for the unglaciated Rupelian (a). Changes in the northward heat flux in response to glaciation are shown for the Priabonian (b) and Rupelian (c), and changes in response to gateway opening (unglaciated Rupelian – unglaciated Priabonian) are shown in (d). In all figures, black lines show total, red lines show atmospheric and blue lines show oceanic heat fluxes.

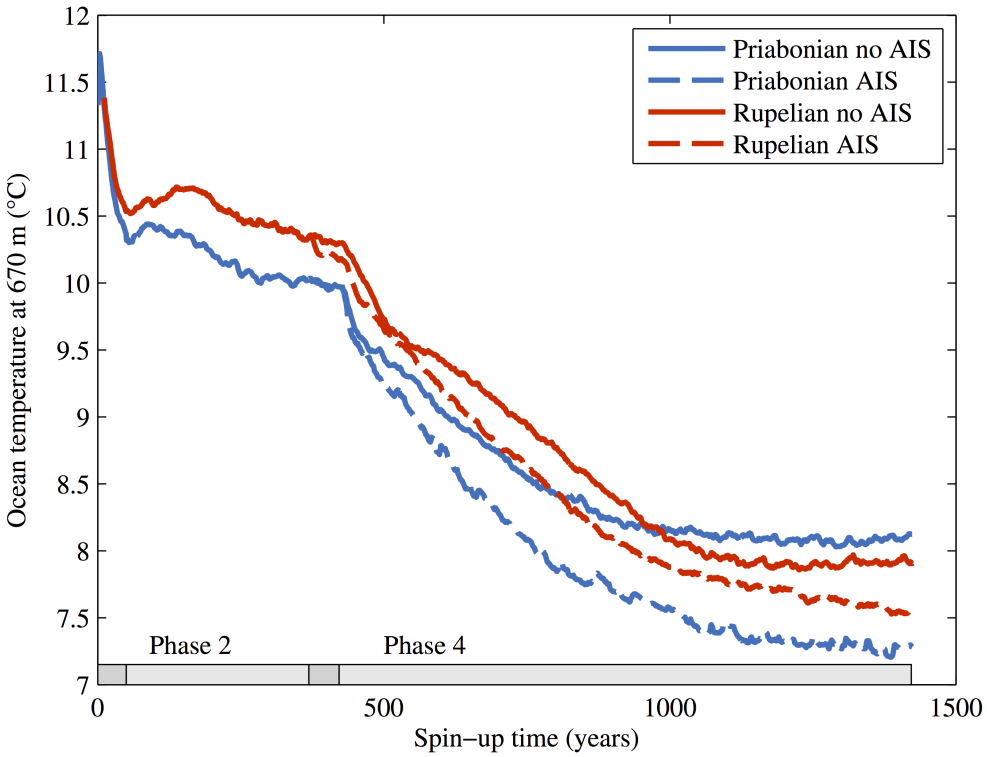

Figure S1: Model spin-up trends of mean ocean temperature at 670 m depth (°C) for the four main simulations. The four phases of spin-up (detailed in section 2) are indicated by the grey bars.

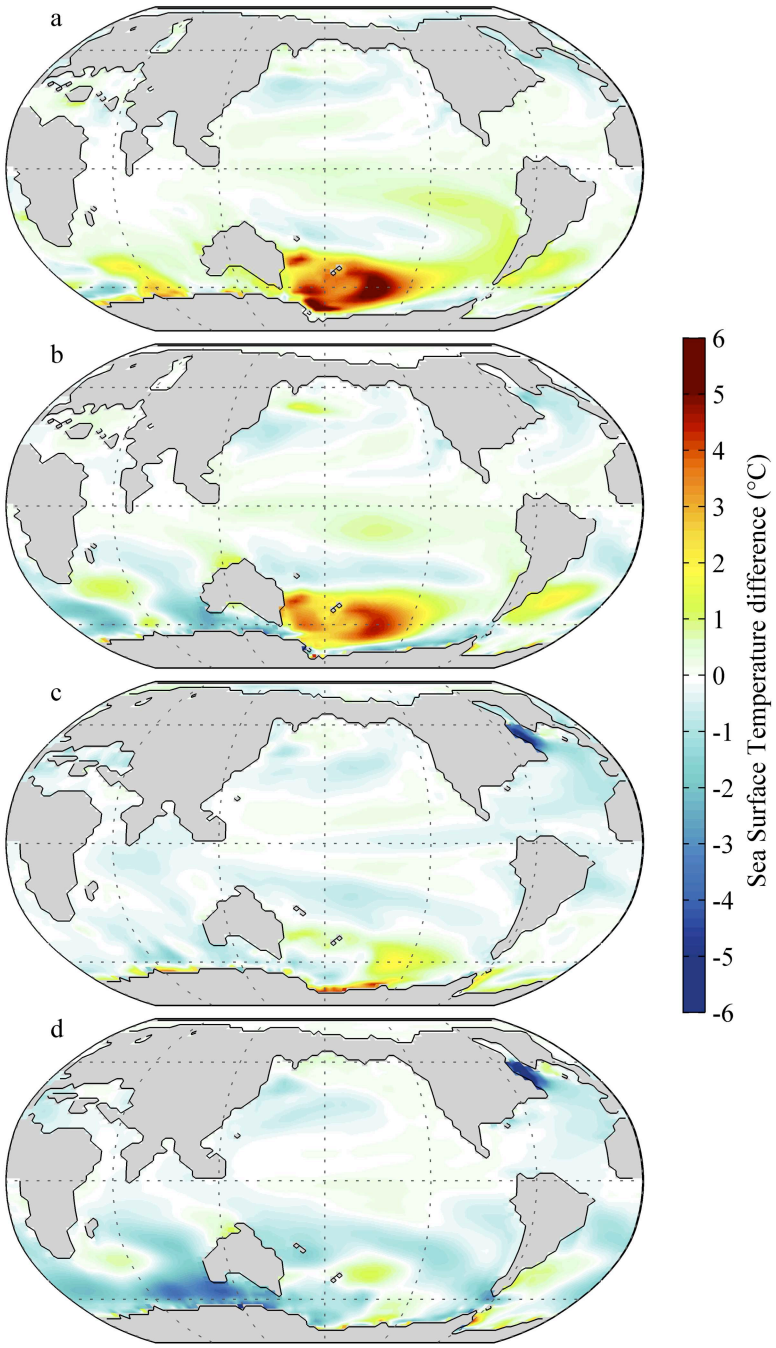

Figure S2: Seasonal mean sea surface temperature response to Antarctic glaciation (°C) for the Priabonian winter (a), Priabonian summer (b), Rupelian winter (c) and Rupelian summer (d). Summer is defined December, January and February; winter is June, July and August.

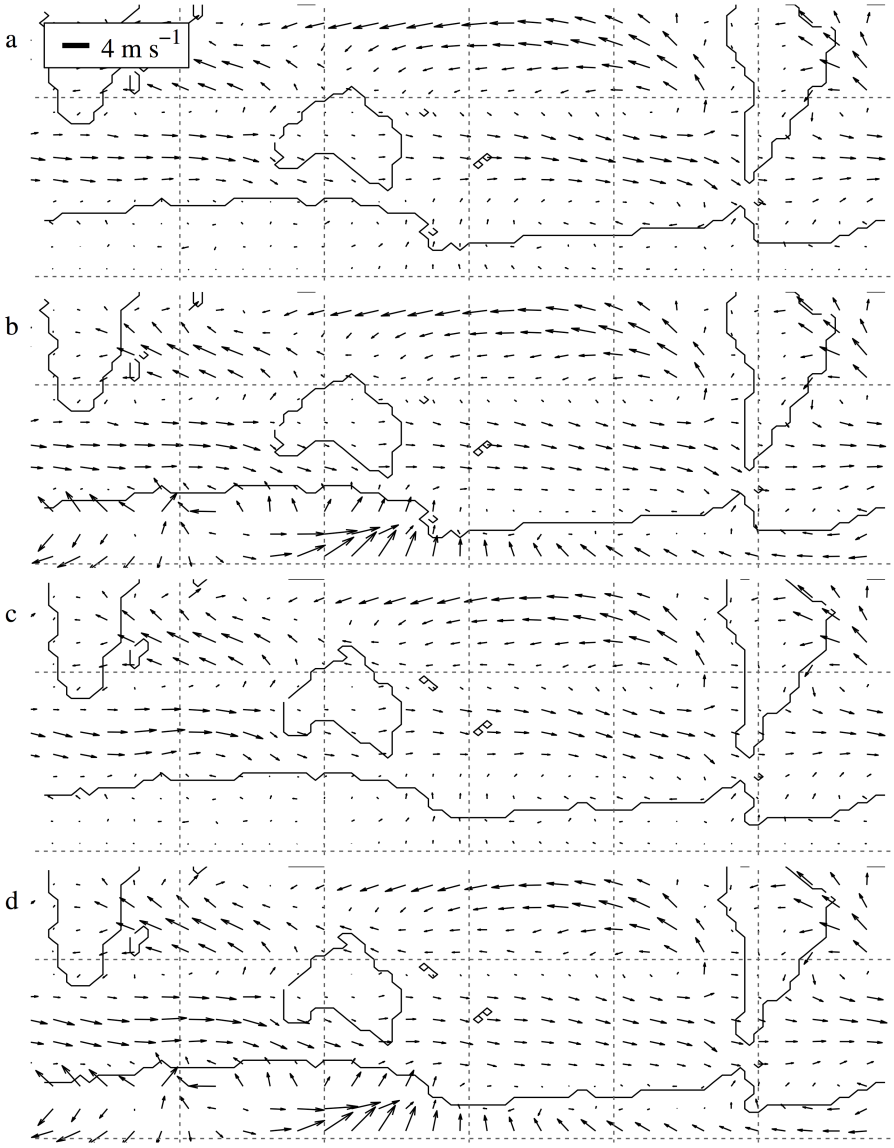

Figure S3: Vectors of Southern Hemisphere surface wind strength (m s^{-1}) for the unglaciated Priabonian (a), glaciated Priabonian (b), unglaciated Rupelian (c) and glaciated Rupelian (d). Vector scale is located in (a).

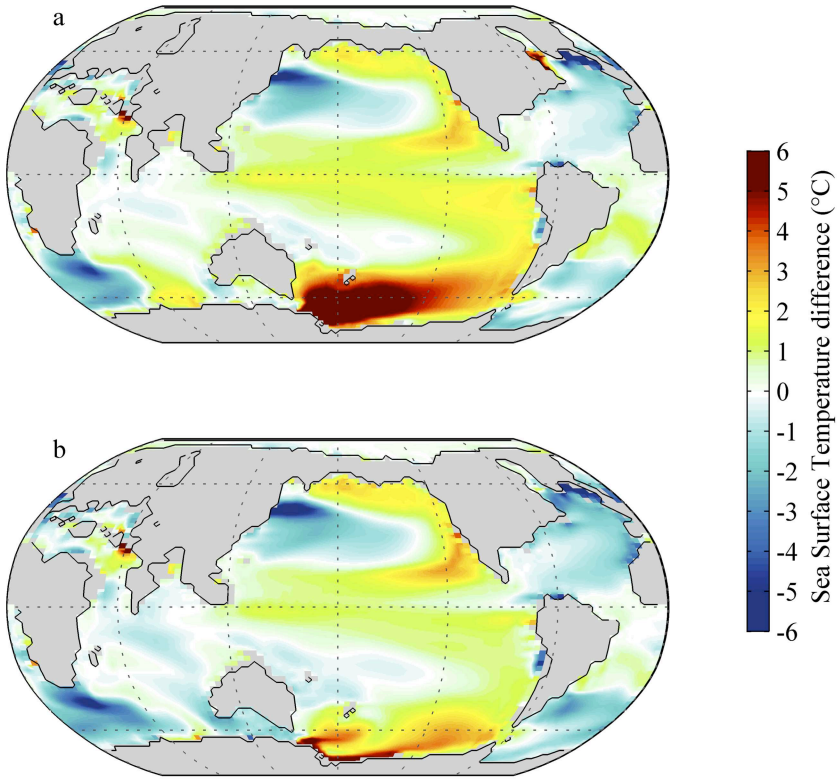

Figure S4: Sea surface temperature difference between the stages for the same ice sheet configuration (°C), shown for the unglaciated Rupelian – unglaciated Priabonian (a) and the glaciated Rupelian – glaciated Priabonian (b).

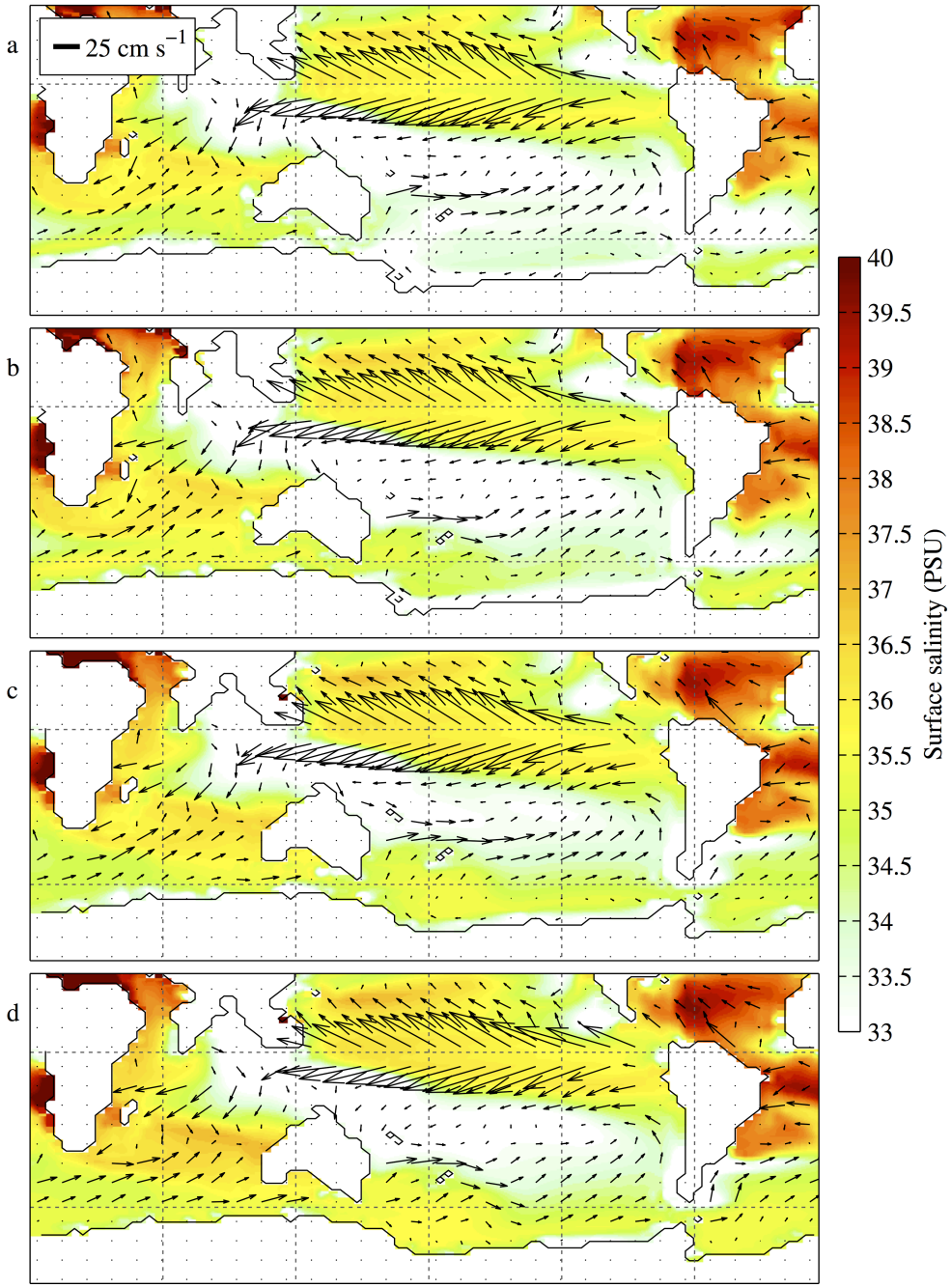

Figure S5: Ocean surface currents (vectors) and sea surface salinity (PSU) for the unglaciated Priabonian (a), glaciated Priabonian (b), unglaciated Rupelian (c) and glaciated Rupelian (d). Vector scale is located in (a).

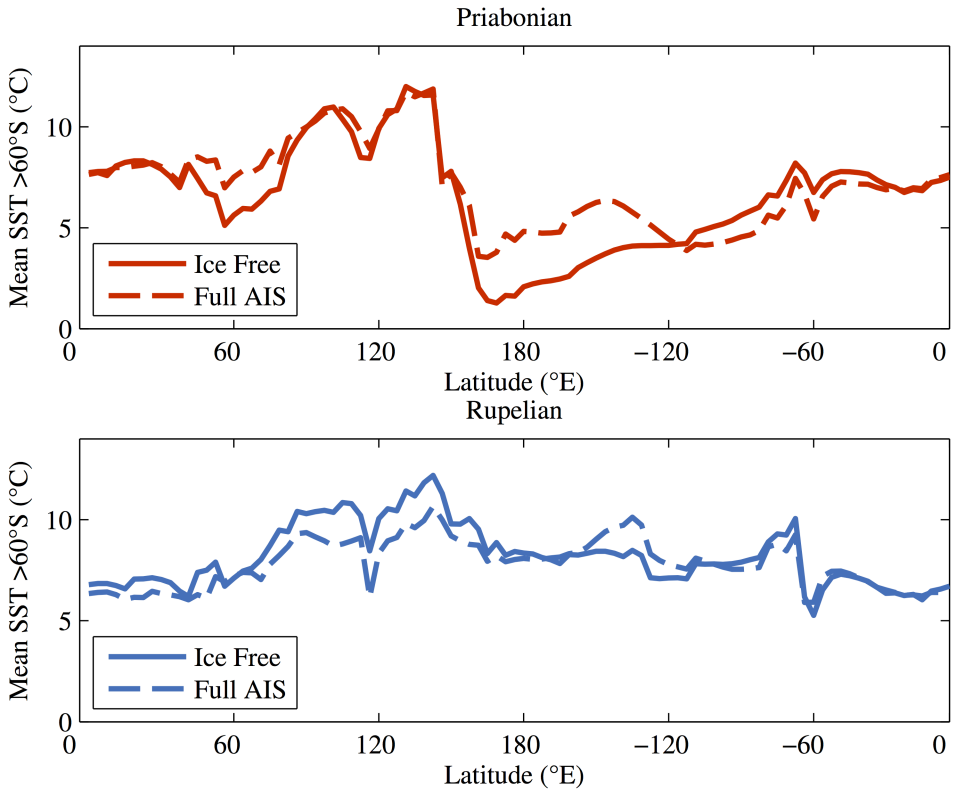

Figure S6: Meridionally averaged sea surface temperature profile (°C) for the Southern Ocean (>60 °S). The Priabonian is shown in red and the Rupelian in blue. The solid lines show the unglaciated and the dashed lines the glaciated simulations.